Accepted Manuscript

The compressive properties of sandwich structures based on an egg-box core design

A. Haldar, Z. Guan, W.J. Cantwell, Q.Y. Wang

PII: S1359-8368(18)30033-7

DOI: 10.1016/j.compositesb.2018.03.007

Reference: JCOMB 5566

To appear in: *Composites Part B*

Received Date: 4 January 2018

Revised Date: 21 February 2018

Accepted Date: 3 March 2018

Please cite this article as: Haldar A, Guan Z, Cantwell WJ, Wang QY, The compressive properties of sandwich structures based on an egg-box core design, *Composites Part B* (2018), doi: 10.1016/j.compositesb.2018.03.007.

The compressive properties of sandwich structures based on an egg-box core design

A. Haldar[1], Z. Guan* [1,2], W.J. Cantwell[3] and Q.Y. Wang[2]

[1] School of Engineering, University of Liverpool, Liverpool L69 3GH, UK.

[2]School of Mechanical Engineering, Chengdu University, Chengdu 610106, China

[3] Department of Aerospace Engineering, Khalifa University, Abu Dhabi, United Arab Emirates.

Abstract

Lightweight cores, based on an egg-box core design, have been manufactured using a simple compression-moulding technique. Two types of composite prepreg were used to manufacture the core materials, these being a woven carbon fibre reinforced epoxy and a woven glass fibre reinforced epoxy. The resulting cores were of a high quality, exhibiting little or no wrinkling following the manufacturing procedure. Subsequent compression tests at quasi-static rates of loading showed that the compression strength of the core depended strongly on the level of constraint applied during testing, with sandwich panels based on composite skins bonded to an egg-box core offering a load-bearing capability that was more than double that of its unconstrained counterpart. The quasi-static compression strength of the carbon-based cores has been shown to be slightly higher than the glass fibre systems, particularly at higher core densities. Local splitting damage at cell joining regions and crushing of the cell of the egg-box structure was identified as the primary failure mechanism in the sandwich panels.

Impact tests, conducted using a drop-weight impact tower, have shown that the compression strength of the egg-box cores is higher at dynamic rates of loading than at quasi-static rates. Here again, the local splitting and crushing was the primary mode of failure in the sandwich structures. Finally, the finite element technique has been used to model the mechanical response of these core designs under both quasi-static and impact loading testing conditions. Here, agreement between the predicted and observed responses was found to be good for both extremes of loading-rate.

Keywords: A. Carbon-fibre; A. Glass fibre; B. Impact behaviour; C. finite element analysis (FEA) ; composite egg-box

1. Introduction

Sandwich structures consisting of a low density core material bonded to strong, stiff outer skins are finding increasing deployment across a broad range of engineering applications [1,2]. Such structures offer many unique advantages, most particularly when subjected to out-of-plane loading, such as that associated with the application of bending or flexural loads. Although sandwich technology is now well-established, there have been many attempts in recent years to develop new and novel core designs that can greatly expand the design envelope. Examples include the development of advanced lattice designs that seek to exploit the tensile deformation modes when loaded in compression as well as corrugated structures that offer increased levels of ventilation in humid environments [3-8]. Kazemahvazi et al. [9] investigated the compression behaviour of a corrugated system based on a carbon fibre reinforced epoxy resin. The resulting panels exhibited a number of different failure modes as the geometry of the structure was varied. More recently, corrugated core materials, based on both glass and carbon fibre reinforced epoxy composites, have been developed and tested [10]. Here, the compression moulding technique, employing a steel mould with a triangular profile, was used to produce a range of systems with differing wall thicknesses. The mechanical response of the composite sandwich structures were compared to that offered by an all-aluminium system, where it was shown that the specific compression strength of a carbon fibre-based core exceeded that of its metallic counterpart [10].

Found et al. [11] performed quasi-static compression tests to investigate the energy absorption properties of a polyurethane foam sandwich panel with four fibre-reinforced plastic tubular inserts incorporated within the core. They reported that by ensuring progressive brittle failure of the structure, higher specific energy absorption values were obtained. As a result of variations in the fibre distribution within the inserts, the sandwich tended to collapse in a catastrophic failure mode, leading to lower specific energy values. The energy-absorbing characteristics of hierarchical woven lattice composites were evaluated by Zheng et al. [12]. The square interlocking structures were composed of a woven lattice to form the sandwich cell walls. They concluded that these novel cell walls successfully restricted rib buckling. As a result, the structure had a high compressive strength and a stable plateau region, thereby enhancing the specific energy absorption of the cellular material.

A potential new class of energy-absorbing structure based on aluminium egg box was introduced by Zupan et al. [13]. Experiments suggested that egg-box structures deform by either the rotation of a stationary plastic hinge or by a travelling plastic knuckle, depending upon the in-plane kinematic constraints imposed upon the egg-box. Chung et al. [14] fabricated composite egg-box structures and stated that its density, boundary conditions and geometry affected the energy absorption capability of the structure. Fibre reinforced composite structures were manufactured using vacuum bagging and autoclave curing techniques. The production of foam-filled egg-box sandwiches, via autoclave curing, was investigated by Yoo et al. [15]. It was found that such structures offered an impressive energy absorption capacity, involving a stable collapse response, resembling that of an ideal energy-absorbing material.

Although extensive work has been carried out to understand the effect of various sandwich geometries on energy absorption, there is limited work relating to the mechanical properties of contoured core sandwich panels (or the egg-box structure) based on composite materials. The present study investigates the properties of contoured core sandwich panels based on both carbon and glass fibre composites. The study initially focuses on the quasi-static and impact response of these panels as a function of the cell wall thicknesses and core density. Following this, a series of finite element models are developed to predict the mechanical response of these structures under compression loading.

2. Experimental procedure

The egg-box composite cores investigated in this study were manufactured using either a woven glass fibre reinforced epoxy (GFRP) or a woven carbon fibre reinforced epoxy (CFRP). The nominal thicknesses of the GFRP and CFRP prepregs were 0.10 and 0.25 mm respectively. Details of physical properties of these two prepreg materials are given in Table 1. Prepreg sheets were cut to the required dimensions and placed between the two contoured aluminium moulds shown in Figure 1a. Geometrical details of the mould design are given in Figure 1b. The GFRP cores were manufactured by stacking 5, 10 and 15 prepreg sheets in the mould, and the thicknesses of the resulting cores were 0.5, 1.0 and 1.5 mm respectively. CFRP cores having similar thicknesses were produced by stacking 2, 4 and 6 prepreg sheets in the mould. A release agent (CIL Release 1711E, from Cilchem) was sprayed on both sides of the mould to ensure easy demoulding at the end of the cure cycle. The aluminium moulds were then placed in a hot press and the structure cured according to the processing parameters given in Table 1. Here, the panels were heated to 125 ^{o}C at a heating rate of 1.5 ^{o}C/minute. This temperature was then maintained for 90 minutes, before switching off the press and allowing the samples to cool to room temperature. The panels were then removed from the press and cut into 100 x 100 mm test samples, as shown in Figure 2(a).

To manufacture the bonded samples, skins were bonded to the core using a two-part epoxy resin (Araldite 420 A/B) in the ratio 10:4. All of the cores were bonded to 0.50 mm thick skins based on either CFRP or GFRP. The adhesive was applied to the core using a syringe. After bonding, the panels were cured in an oven at 120 ^{o}C for one hour. The manufactured sandwich panels are shown in Figure 2(b). An examination of the panels showed that they were free of defects, such as wrinkling or warping, suggesting that the weaves offered sufficient drapability to cope with the relatively complex mould design.

In the initial part of this investigation, unbonded plain core specimens (i.e. without skins) were subjected to quasi-static compression using an Instron 4505 universal test machine. Tests were conducted on two by two (100x100 mm) egg-box panels. Following this, a series of compression tests were performed on sandwich panels with similarly-sized cores and corresponding skins. In a number of tests, the lateral movement of the base of the cores was restricted to investigate the influence of boundary conditions on the compression response. All of the quasi-static compression tests were undertaken at a crosshead displacement rate of 1 mm/minute. The crosshead movement was interrupted when the panel was fully crushed between the loading platens. The load-displacements response was converted to nominal stress-strain curves by normalising the applied load by the planar area of the specimen and dividing the crosshead displacement by the original specimen height, respectively. Table 2 summaries the sandwich structures investigated under quasi-static compression loading, which includes ply number, sample dimensions and core density. Here, in specimen ID ‘GF’ represents glass fibre and ‘CF’ represents carbon fibre.

The compression tests were repeated at dynamic rates of loading using a drop-weight impact tower. A flat square impacter (100 mm x 100 mm) with a mass up to 15 kg was dropped onto panels supported on a steel base. The resulting impact force was recorded using a 10 kN piezo-electric load cell (Kistler 9321A) positioned under the steel base. The cell was connected to a charge amplifier (Kistler 5011) using an insulated coaxial cable in order to amplify the resulting voltage signal. The recorded signal was then converted from an analogue to a digital format using a DAQ device (Measurement Computing, USB 1208HS) and then converted to a force. A high speed camera (MotionPro X4, model X4CU-U-4) was used to capture the displacement and velocity of the impactor. The camera was placed in the front of the impact rig to track the impactor and record displacement during the dynamic event, as shown in Figure 3. Table 3 summarises the key parameters used in this part of the study, which include number of ply, cell wall thickness, sample dimensions, core density, drop height and impactor mass.

3. Numerical procedure

Numerical models were developed to simulate the compression response of the sandwich structures under quasi-static and dynamic loading. The composite was modelled using user-defined Hashin’s 3D failure criteria for an anisotropic composite material. Figure 4 shows the finite element mesh of an egg-box core with the top skin removed. Here, the core was meshed using six-noded triangular solid elements, while the composite skins were modelled using eight-noded brick elements, with an interface defined between the former and the latter. The loading platens above and below the panel were meshed using discrete rigid elements. The size of the core corresponds to that used in the experimental study (i.e. 100 x100 mm). Mesh sensitivity was investigated by varying the mesh density within the plane and through-thickness directions of the composite sheet. Following this study, a mesh size based on element with a size of 1 mm within the plane and two elements through-the-thickness of the composite layer was used. A number of interfaces were considered in the model, including those between the face sheets and the loading platen, those between the composite core and the face sheets, as well as possible self-contact between the inclined faces of the egg-box core. A modified 3D failure criteria [16, 17] was used to simulate the response of sandwich panels in a Cartesian coordinate system. The failure criteria, together with the related constitutive model, were then implemented in ABAQUS/Explicit using a subroutine [18, 19]. The failure criteria can be expressed as follows:

Fibre tension: $(\sigma_{11} > 0)$

$$F_f^t = \left(\frac{\sigma_{11}}{X_{1t}}\right)^2 + \left(\frac{\sigma_{12}}{S_{12}}\right)^2 + \left(\frac{\sigma_{13}}{S_{13}}\right)^2,\ d_{ft} = 1 \qquad (1)$$

Fibre compression: $(\sigma_{11} < 0)$

$$\frac{|\sigma_{11}|}{X_{1t}}, d_{fc} = 1,\ d_{fc} = 1 \qquad (2)$$

Matrix tension: $(\sigma_{22} + \sigma_{33} > 0)$

$$\frac{(\sigma_{22}+\sigma_{33})^2}{X_{2t}^2} + \frac{\sigma_{23}^2 - \sigma_{22}\sigma_{33}}{X_{23}^2} + \frac{\sigma_{12}^2 + \sigma_{13}^2}{X_{12}^2} = 1,\ d_{mt} = 1 \qquad (3)$$

Matrix compression: $(\sigma_{22} + \sigma_{33} < 0)$

$$\left[\left(\frac{X_{2c}}{2S_{23}}\right)^2 - 1\right]\frac{(\sigma_{22}+\sigma_{33})}{X_{2c}^2} + \frac{(\sigma_{22}+\sigma_{33})^2}{4S_{23}^2} + \frac{\sigma_{23}^2 - \sigma_{22}\sigma_{33}}{X_{23}^2} + \frac{\sigma_{12}^2 + \sigma_{13}^2}{X_{12}^2} = 1,\ d_{mc} = 1 \qquad (4)$$

where X_{1t}, X_{1c}, X_{2t}, X_{2c}, S_{12}, S_{13} and S_{23} are the various strength components and d_{ft}, d_{fc}, d_{mt} and d_{mc} are the damage variables associated with the four failure modes. A series of numerical studies, with different durations, was conducted in order to identify the appropriate time-step that gave negligible dynamic effects. This time-step was found to be 0.1 seconds. The response of the material after damage initiation, which describes the rate of degradation of the material stiffness once the initiation criterion is satisfied, is defined by the equation:

$$\sigma_{ij} = C_{ij}(d) \cdot \varepsilon_{ij} \qquad (5)$$

where $C_{ij}(d)$ is the degradation matrix. The instant damage criteria are used here, i.e. the damage variables are either taken as zero (virgin state) or unity (damaged state). Therefore, the degradation matrix components are computed in terms of undamaged elastic constants, C_{ij}^{o}, and the damage variables as follows:

$$C_{ij}(d) = (1 - d_{ij})C_{ij}^{o} \quad (6)$$

Here, the damage variable 'd_{ij}' is related to fibre and matrix damage in tension and compression, as well as shear failure in matrix caused by tension and compression, which can have various forms.

The response of the sandwich structures under dynamic loading was modelled using the same elements that were employed in the quasi-static models. The impactor was modelled as a flat plate using a discrete rigid surface. A point mass, equal to that of the experimental impactor, was assigned to a reference point located at the centre of the flat plate. The reference point was also used to record the displacement from this model. An initial velocity was prescribed to the rigid plate, which was set equal to the impact velocity used in the experiments. A surface-to-surface contact condition was used to define contact between the impactor and the skin (so as the core if the skin is damaged).

The input data for the elastic properties and for progressive damage development in this model were based on the properties given in Table 4. A numbers of studies have shown that increased strain-rates, can result in enhanced mechanical properties of composite materials [20-23]. It is generally accepted that the sensitivity of mechanical properties at high-strain rate is dependent on the composite type and polymer matrix.

4. Results and discussion

4.1 The effect of local constraint on the compression response of the cores

The mechanical properties of composite cores similar to those under investigation in this study clearly depend on the level of constraint applied to their boundaries, including the upper and lower surfaces as well as at their edges. Figure 5 shows typical stress-strain plots following compression tests on egg-box cores subjected to three different boundary conditions. Here, the stress and strain are nominal ones, which are defined in Section 2 Experimental Procedure. As expected, the plain unbonded core exhibits a relatively low compressive modulus, as well as a modest compressive strength. Following the initial peak in the curve, the stress drops before rising slowly and dropping on a number of subsequent occasions. An examination of the samples during failure highlighted local splitting at cell joining regions and crushing of the cell, general flattening of the core, delamination between the layers of the composite and finally fracture across the fibres had high levels of compressive strain. Constraining the lateral movement of the edges of the samples yielded a 40% increase in the average peak stress from the unbonded sample. The ensuing collapse and crushing processes resulted in a much higher value of average stress and greater energy absorption, defined by the area under the stress-strain curve, than in the unbonded (unconstrained) sample. Here, mid-way through the crushing process, the nominal stress reached a value similar to that of the initial peak. The failure mechanisms in the constrained samples again involved local splitting at cell joining regions and crushing of the cell prior to complete collapse. Finally, the sandwich panel with composite skins bonded to the composite core offered the highest compression strength of the three conditions investigated here, with the peak value being approximately 2.3 times of that measured on the plain, unconstrained core. Following the peak value, the stress dropped rapidly to values that were significantly lower than those associated with the constrained (bonded) core. The failure modes observed during the damage process in the sandwich panels included local crushing of the core, fibre fracture, delamination between the plies in the core material and debonding at the skin-core interface.

4.2 Compression properties of the sandwich panels

Figures 6(a) and 6(b) show typical stress-strain traces for the GFRP and CFRP sandwich panels respectively. In Figure 6(a), all three traces exhibit an initial linear response up to the peak stress. The peak stress increases with web thickness, ranging from 0.44 MPa for the 0.5 mm web to 1.60 MPa for the 1.5 mm thick web. Following the peak in the trace, a crack initiated in core cell wall, which propagated under continued loading, resulting in steady load drops as the cells collapsed and subsequently crushed. Following this, the core cell wall started to buckle, leading to a sudden drop in stress at strains between 0.1 and 0.2 mm/mm. Beyond a strain of approximately 0.2 mm/mm, the curves plateaued, as the cell walls debonded from the skin, core flattened between the platens. Finally, the stress begins to increase at high strains as the core begins to densify between the platens.

In Figure 6(b), there is again a linear increase over the initial portion of the stress-strain trace of CFRP panels. The maximum stress increases from 0.46 MPa for the 0.5 mm thick web, to 1.61 MPa for its 1.5

mm thick counterpart. A comparison with Fig 6(a) indicates that the strength of the CFRP core is slightly higher than that measured on the GFRP core. Following the peak in trace, the drop in stress is smoother than for the GFRP core. The drop in stress for the 1.0 and 1.5 mm thick systems is continuous until the densification threshold is reached.

Figure 7 summarises the variation of the quasi-static compression stress with core density for the glass and carbon-based sandwich structures, where it is clear that the stress of both materials increases in a roughly linear manner. Here, the core density is defined as the mass of the core divided by the core volume (including cavities). For the lowest density, the strengths are similar, however as density is increased, the superior properties of the CFRP core become apparent.

Figures 8(a) and 8(b) compare the results of the finite element predictions with the data from the experimental traces. Agreement between the two sets of curves is generally good for the GFRP panels, with the model accurately predicting the trends in the experimental results. The model accurately predicts the initial slope, i.e. the elastic modulus of the core, but slightly over-predicts the subsequent softening phase following the peak stress. The oscillations in the predicted traces are due to the unstable response during local collapse in the FE models. Figure 9 presents a comparison of the predictions of the finite element model with the experimentally-measured compression strengths for the CFRP panels. Agreement between the two sets of data is good, suggesting that the numerical model can be used to predict the compression response of structures similar to those tested here. Similar levels of agreement were observed following comparisons between the predicted and measured properties for the GFRP system.

Figure 10 compares the failure mechanisms in the GFRP samples with the predictions offered by the FE model. Agreement between the predictions and experimental data is generally good, with the model predicting local crushing in the core as well as flattening of the core against the upper and lower skins. The model also predicts the final increase in stress due to densification. Agreement between the FE predictions and the experimental curves is also very good for the CFRP panels. Once again, the model accurately captures the initial elastic response, as well as the post-peak softening response of the core. Here, the softening portion of the stress-strain trace is somewhat smoother than observed for the GFRP core.

Figure 11 compares the quasi-static compressive strengths of the CFRP or GFRP egg-box cores with corresponding data for a number of plain foams. From the figure it is evident that the properties of the egg-box cores lie between those associated with linear PVC foams and crosslinked PVC foams. This overall performance is somewhat disappointing given that the current systems are based on composite materials rather than foamed polymers. This relatively modest performance can be attributed to the fact that the composite systems fail at relatively low load levels, due to local crushing in the composite cores.

4.3 The Impact response of the core materials

Figures 12(a) and 12(b) show typical impact traces for the GFRP and CFRP sandwich panels respectively. The GFRP curves exhibit oscillations, due to ringing effects in the load-cell. The curves are similar in form to those following quasi-static testing. As expected, the maximum stress increases with web thickness, passing from approximately 0.44 MPa for the thinnest web to 1.94 MPa for the 1.5 mm thick system. There is evidence to suggest that the onset of densification occurs at lower strains under impact than at quasi-static rates. The dynamic response of the CFRP sandwich structures is similar to the quasi-static traces. Once again, the stress in the thickest sample drops steadily from the peak value. Here, the peak stress for the 1.5mm thick CFRP panel is 2.20 MPa, compared to 0.77 MPa for the 0.5 mm thick CFRP panel.

Figure 13 compares the dynamic and quasi-static compression strengths of the GFRP sandwich structures. It is interesting to note that for the two thinner webs, the compression strength of the dynamically-loaded samples is similar to those of their quasi-static counterparts. In contrast, loading-rate effects are evident in the thickest system, with the dynamic value being 35% higher than the quasi-static system. Figure 13(b) presents the dynamic and quasi-static properties of the CFRP sandwich panels. Here, there is evidence of loading-rate sensitivity, with the impact strength of both the thinnest and thickest webs being up to 25% higher than at quasi-static rates.

Figure 14 compares the stress-strain responses predicted by the FE models with the experimental traces for the CFRP panels. As before, the FE model exhibits a highly oscillatory response for all web thicknesses. A comparison of the numerical and experimental traces indicates that the finite element model captures the fundamental features of the experimental stress-strain traces. However, following the initial peak in the stress-strain traces the FE model tends to over-predict the softening phase of the curves.

Figure 15 compares the FE predictions of the compression strength of the GFRP sandwich panels with the experimental data where good agreement between the two sets of data is apparent. Similar trends were observed when the predictions and experimental data for the CFRP samples are compared, although the model tended to slightly over-estimate the measured values. This evidence further supports the argument that the finite element model is suitable for predicting the dynamic behaviour of these relatively complex sandwich structures.

5. Conclusions

A range of egg-box composite cores have been manufactured via a compression moulding process in a hot press. Compression tests at quasi-static and dynamic loading-rates have identified a range of failure modes, including flattening of the core webs, local crushing of the cell and delamination within the cell walls, followed by the debonding between core and skins. The influence of edge constraint has been studied, where it was noted that sandwich structures based on composite skins bonded to an egg-box core offered the highest compression strength. Increasing the thickness of the web in the egg-box core served to increase the compression strength, although failure always occurred as a result of delamination and local crushing in the relatively thin inclined faces of the inclined core members. The compression properties of both materials exhibit a degree of loading-rate sensitivity, with GFRP being slightly more loading-rate sensitive than its carbon-based counterpart. Finite element models, developed to predict the quasi-static and dynamic compression behaviour of the egg-box cores, have shown a reasonably good agreement with the experimental data.

Acknowledgements

The authors would like to thank the Government of India to provide the PhD Scholarship to financially support this research work.

References

[1]. L. J. Gibson and M. F. Ashby, Cellular solids: Structure and Properties. Cambridge University Press, Cambridge, 1997.

[2]. M. Daniel and O. Ishai, Engineering Mechanics of Composite Materials, Oxford University Press, 1994.

[3]. D. T. Queheillalt and H. N. G. Wadley, Pyramidal lattice truss structures with hollow trusses, Materials Science and Engineering A, 397, 2005, pp132–137.

[4]. F. W. Zok, H. J. Rathbun, Z. Wei, and A. G. Evans, Design of metallic textile core sandwich panels, International Journal of Solids and Structures, 40, 2003, pp5707–5722.

[5]. S. Chiras, D. R. Mumm, A. G. Evans, N. Wicks, J. W. Hutchinson, K. Dharmasena, H. N. G. Wadley and S. Fichter, The structural performance of near-optimized truss core panels, International Journal of Solids and Structures, 39, 2002, pp4093–4115.

[6]. J. Wang, A. G. Evans, K. Dharmasena and H. N. G. Wadley, On the performance of truss panels with Kagome cores, International Journal of Solids and Structures, 40, 2003, pp6981–6988.

[7]. J. Xiong, B. Wang, L. Ma, J. Papadopoulos, A. Vaziri and L. Wu, Three-dimensional composite lattice structures fabricated by electrical discharge machining: Experimental mechanics, 54, 2013, pp405–412.

[8]. S. Yin, L. Wu and S. R. Nutt, Compressive efficiency of stretch-stretch-hybrid hierarchical composite lattice cores, Materials and Design, 56, 2014, pp731–739.

[9]. S. Kazemahvazi, D. Tanner and D. Zenkert, Corrugated all-composite sandwich structures. Part 2: Failure mechanisms and experimental programme, Composites Science and Technology, 69, 2009, pp920-925.

[10]. M. R. M. Rejab and W. J. Cantwell, The mechanical behaviour of corrugated-core sandwich panels, Composites. Part B Engineering, 47, 2013, pp267–277.

[11]. M.S. Found, A.M. Robinson, and J.J. Carruthers, The influence of FRP inserts on the energy absorption of a foam-cored sandwich panel, Composite Structures, 38, 1997, pp373–381.

[12]. J. Zheng, L. Zhao and H. Fan, Energy absorption mechanisms of hierarchical woven lattice composites, Composites: Part B, 2012; 43: 1516 – 1522.

[13]. M. Zupan, N. Fleck, and M. Ashby, "The collapse and energy absorption of egg-box panels," in Proceedings of the 3rd TMS Annual Meeting and Exhibition, 2002, pp243-250.

[14]. J. Chung, S. Chang, and M. Sutcliffe, Deformation and energy absorption of composite egg-box panels, Composites Science and Technology, 67, 2007, pp2342-2349.

[15]. S. Yoo, S. Chang, and M. Sutcliffe, Compressive characteristics of foam-filled composite egg-box sandwich panels as energy absorbing structures, Composites Part A: Applied Science and Manufacturing, vol. 41, 2010, pp427-434.

[16]. Z. Hashin, Failure criteria for unidirectional fiber composites, Journal of Applied Mechanics, 1980;(47):329–334.

[17]. E. Sitnikova, Z.W. Guan, G.K. Schleyer, W.J.Cantwell, Modelling of perforation failure in fibre metal laminates subjected to high impulsive blast loading, International Journal of Solids and Structures. 2014; (51): 3135-3146.

[18]. T. P. Vo, Z. W. Guan, W. J. Cantwell, G. K. Schleyer. Modelling of the low-impulse blast behaviour of fibre–metal laminates based on different aluminium alloys, Composites: Part B, 2013; (44): 141–151.

[19]. J. Zhou, Z. W. Guan, W. J. Cantwell, Modeling of the compression behavior of foam cores reinforced with composite rods, Polymer Composites 09/2015; DOI:10.1002/pc.23812.

[20]. M. I. Alam and S. Fawzia, "Numerical studies on CFRP strengthened steel columns under transverse impact," Composite Structures, vol. 120, pp. 428-441, 2015.

[21]. J. Harding and L. M. Welsh, "A tensile testing technique for fibre-reinforced composites at impact rates of strain," Journal of Materials Science, vol. 18, pp. 1810-1826, 1983.

[22]. D. F. Adams and D. G. Adams, "Tensile impact tests of AS4/3501-6 and S2/3501-6 unidirectional composites and the 3501-6 epoxy matrix," Journal of Composite Materials, vol. 24,256-268, 1990.

[23]. H. Al-Zubaidy, X.-L. Zhao, and R. Al-Mahaidi, "Mechanical characterisation of the dynamic tensile properties of CFRP sheet and adhesive at medium strain rates," Composite Structures, vol. 96,153-164, 2013.

Table 1. Details of the glass fibre and carbon fibre reinforced epoxy composites

Prepreg	GFRP	CFRP
Fibre type	E-Glass	3k HTA
Weave style	Satin	Plain
Resin content (% wt)	40 ± 3	53 ± 3
Curing temperature (^{o}C)	125	125
Dwell time (minutes)	90	90
Laminate density (kg/m^3)	1780	1300
Nominal thickness of ply (mm)	0.10	0.25

Table 2. Summary of the dimensions of the sandwich structures investigated at quasi-static rates of strain.

Specimen ID	No. of plies	Thickness 't' (mm)	Specimen Length (mm)	Specimen Width (mm)	Specimen Height (mm)	Core density (kg/m^3)
GF1	5	0.5	100	100	20.5	54.5
GF2	10	1.0	100	100	21.0	104.3
GF3	15	1.5	100	100	21.5	141.3
CF1	2	0.5	100	100	20.5	50.1
CF2	4	1.0	100	100	21.0	97.4
CF3	6	1.5	100	100	21.5	130.3

Table 3. Summary of the dimensions of the sandwich structures and test parameters for low velocity impact testing.

Specimen ID	No. of plies	Thickness 't' (mm)	Specimen Length (mm)	Specimen Width (mm)	Specimen Height (mm)	Core density (kg/m^3)	Drop height (m)	Impactor mass (kg)
GF4	5	0.5	100	100	20.5	54.5	0.40	8.43
GF5	10	1.0	100	100	21.0	104.3	0.85	8.43
GF6	15	1.5	100	100	21.5	141.3	1.40	8.43
CF4	2	0.5	100	100	20.5	50.1	0.50	15.70
CF5	4	1.0	100	100	21.0	97.4	1.10	15.70
CF6	6	1.5	100	100	21.5	130.3	1.45	15.70

Table 4. Summary of material properties of two composites used in this study.

Properties	Symbol	(GFRP)	(CFRP)
Young’s modulus in longitudinal direction	E_{11}	23 GPa	48 GPa
Young’s modulus in transverse direction	E_{22}	23 GPa	48 GPa
Young’s modulus in thickness	E_{33}	5 GPa	1 GPa
In-plane shear modulus	G_{12}	5 GPa	9 GPa
Through-thickness shear modulus	G_{13}, G_{23}	5 GPa	9 GPa
In-plane Poisson’s ratio	v_{12}	0.15	0.10
Through-thickness Poisson’s ratio	v_{13}, v_{23}	0.15	0.10
Longitudinal tensile strength	T_L	320 MPa	550 MPa
Longitudinal compressive strength	C_L	260 MPa	150 MPa
Transverse tensile strength	T_T	320 MPa	550 MPa
Transverse compressive strength	C_T	260 MPa	350 MPa
Transverse shear strength	S_T	100 MPa	120 MPa
Longitudinal shear strength	S_L	100 MPa	120 MPa

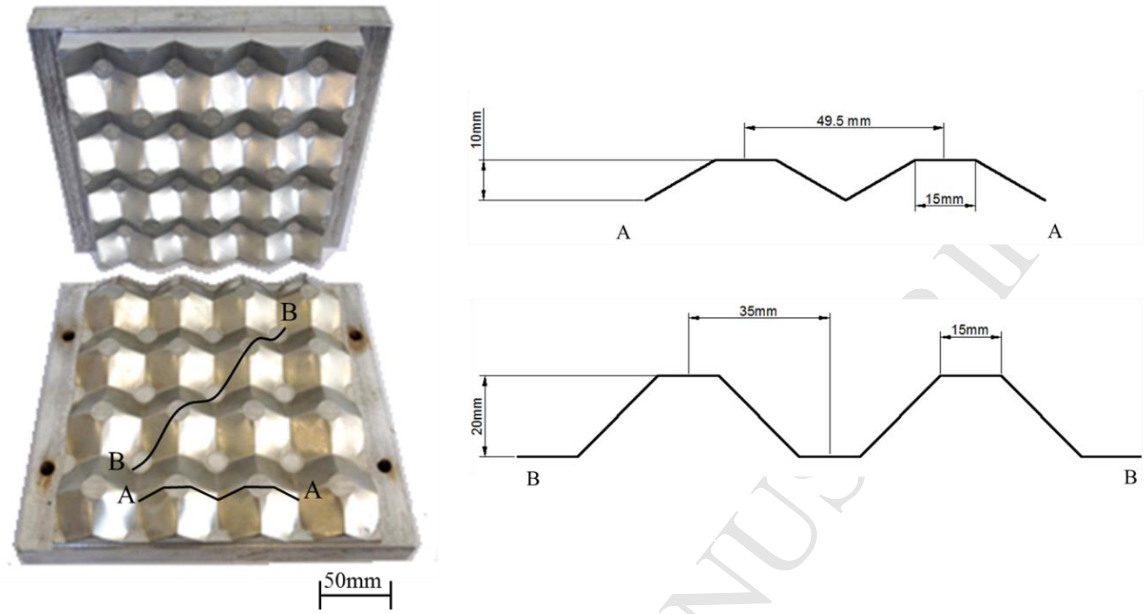

(a) (b)

Figure 1. Photographs of the mould and profile of the mould showing the egg-box design.

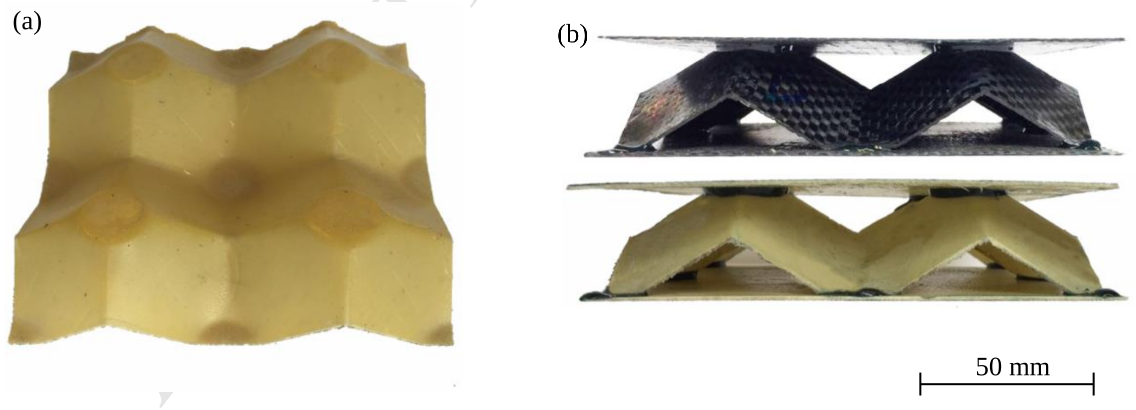

Figure 2. Photograph of (a) a GFRP core after manufacture and (b) the resulting CFRP and GFRP sandwich structures based on composite skins bonded to the core.

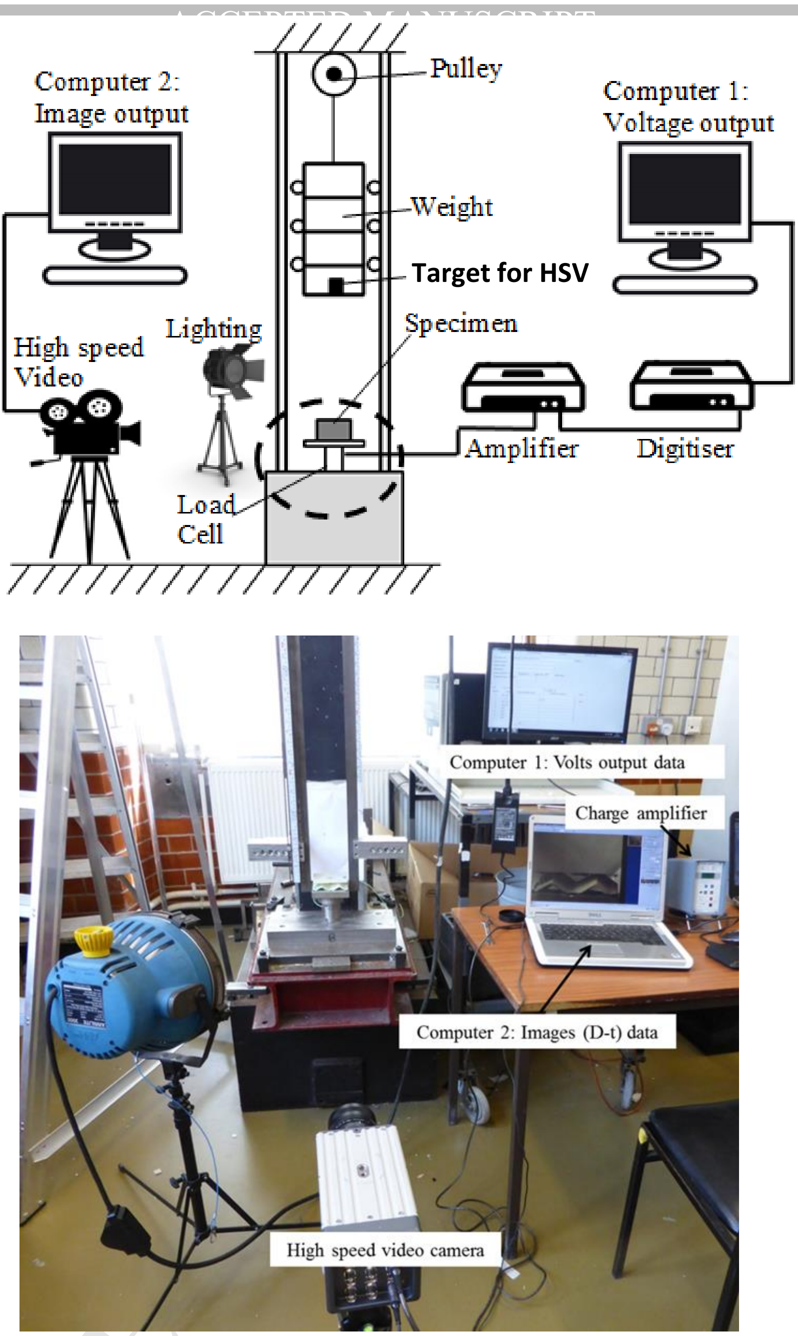

Figure 3. Schematic and image of the drop-weight impact tower.

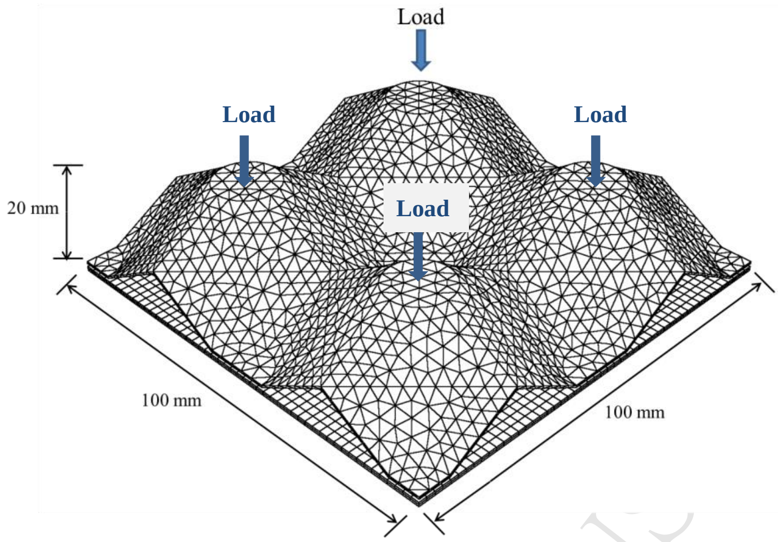

Figure 4. Finite element mesh of the egg-box model.

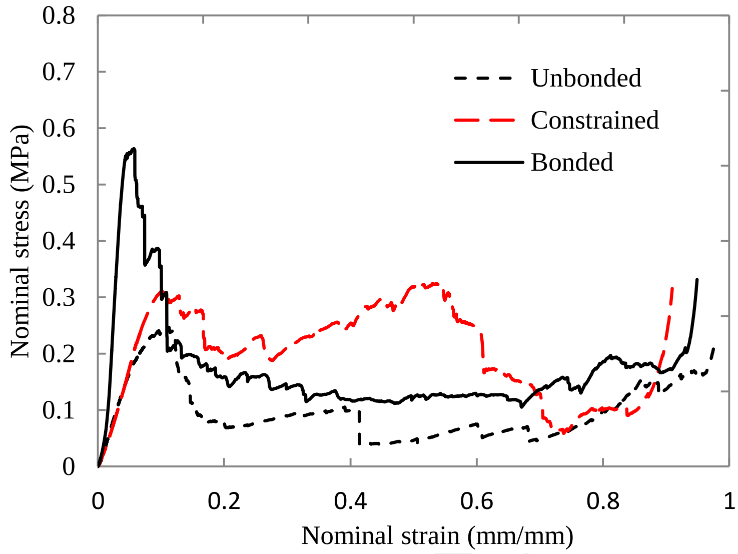

Figure 5. The effect of edge constraint and skins (bonded) on the compression response of the GFRP system.

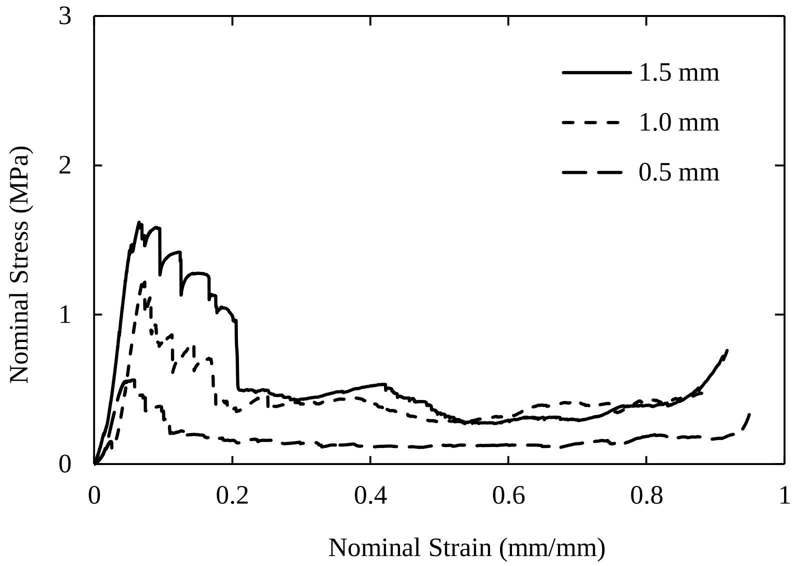

(a)

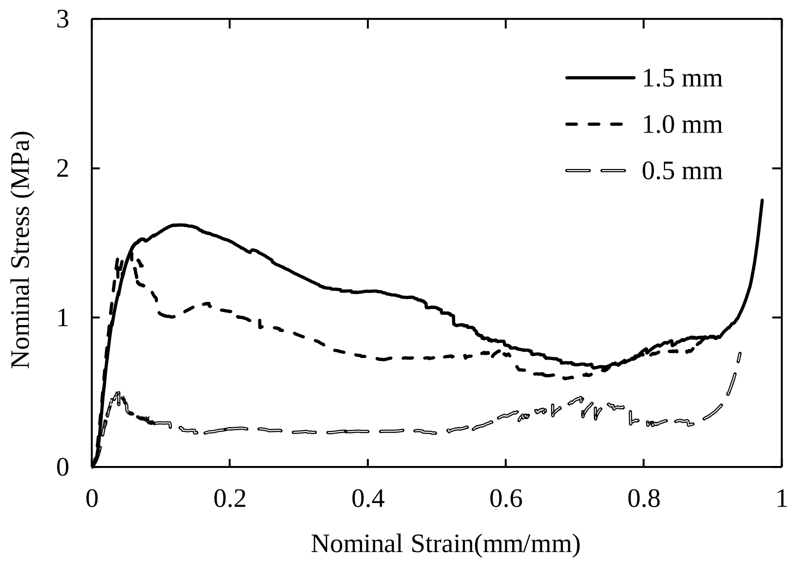

(b)

Figure 6. Typical stress-strain traces following quasi-static compression tests on (a) the GFRP sandwich panels and (b) the CFRP sandwich panels.

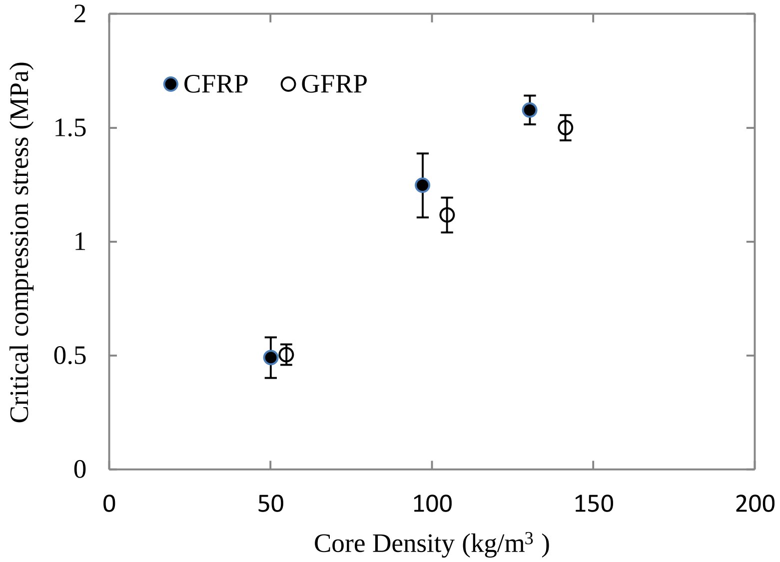

Figure 7. Variation of compression strength with core density for the GFRP and CFRP panels.

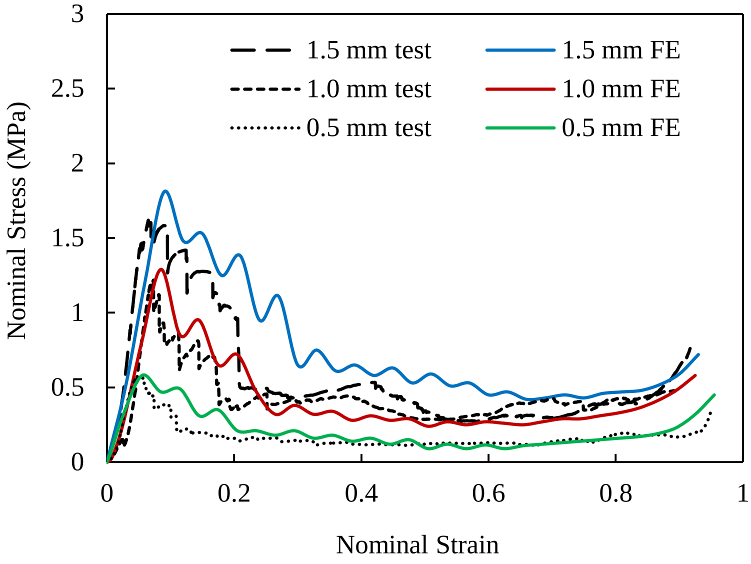

(a) GFRP

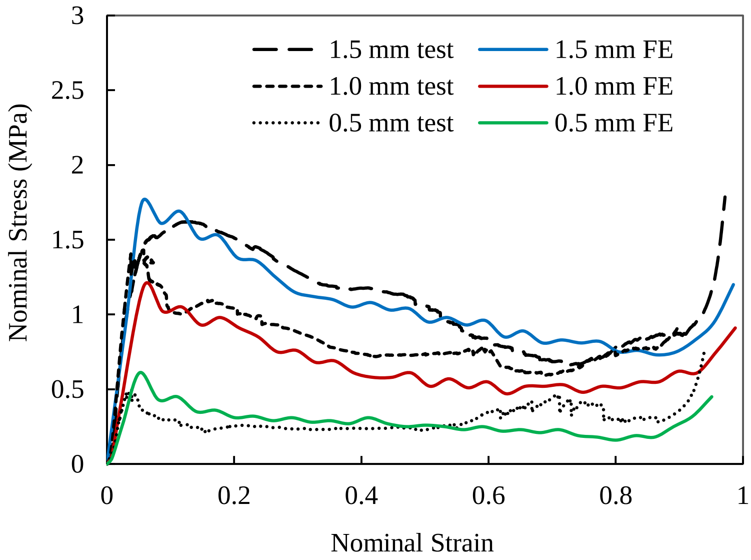

(b) CFRP

Figure 8. Comparison of the numerical and experimental stress-strain traces for the GFRP and CFRP cores.

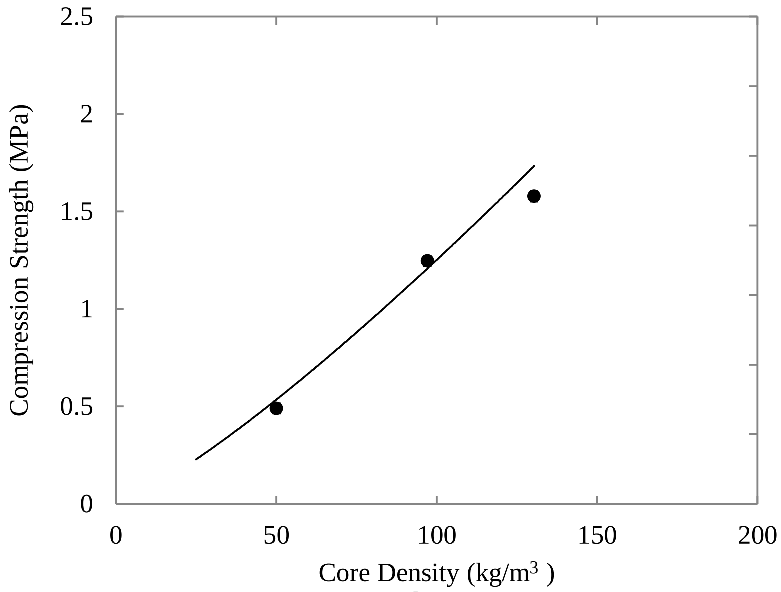

Figure 9. Quasi-static compression strength versus core densities for the CFRP sandwich structures. The solid line correspond to the FE predictions.

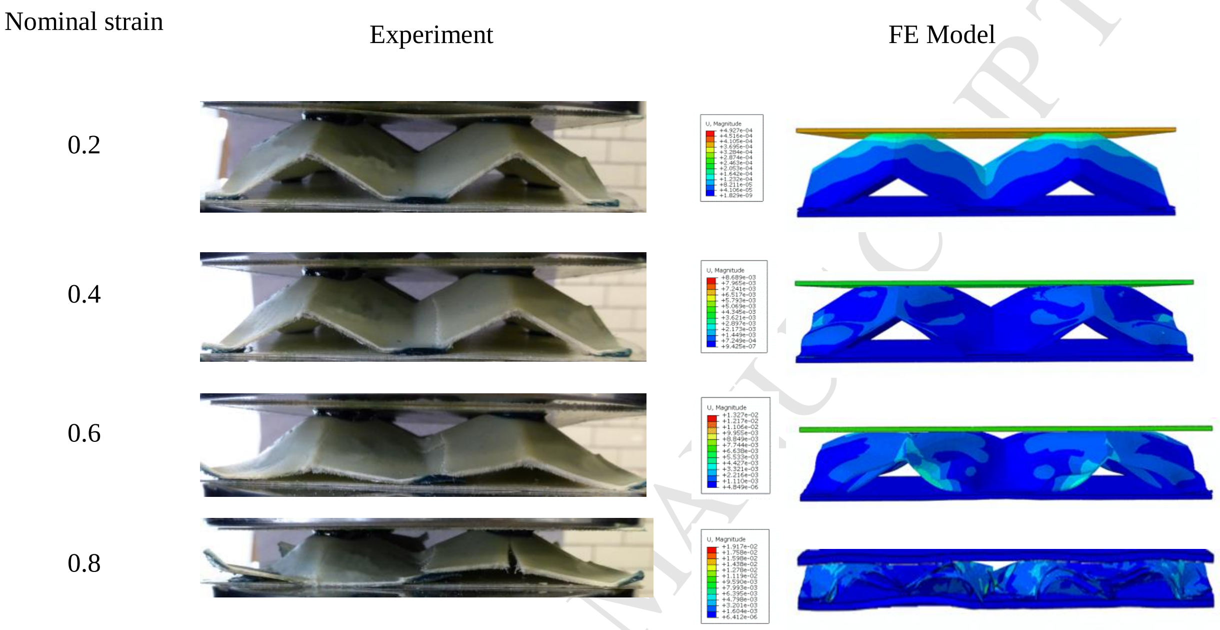

Figure 10. Photographs showing the compression process in the flat roof GFRP structures (a) experimental observation and (b) finite element predictions.

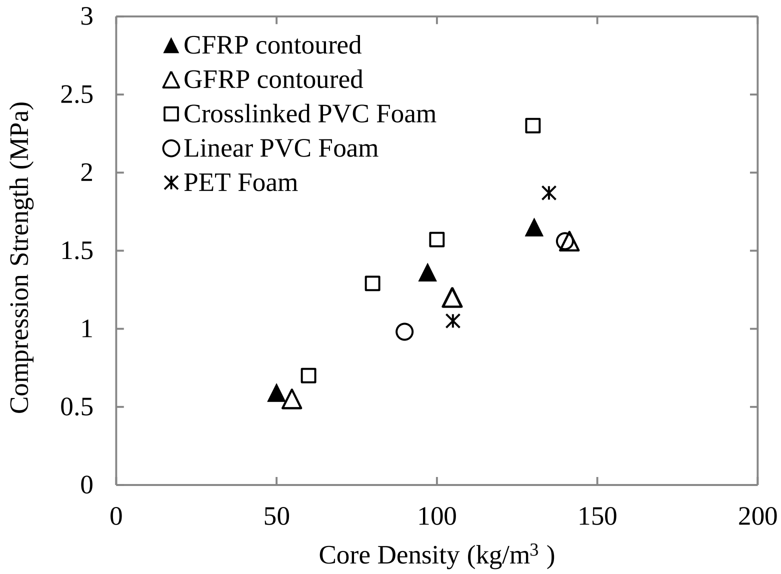

Figure 11. Comparison of the compression strength of the egg box cores with other core types as a function of core density.

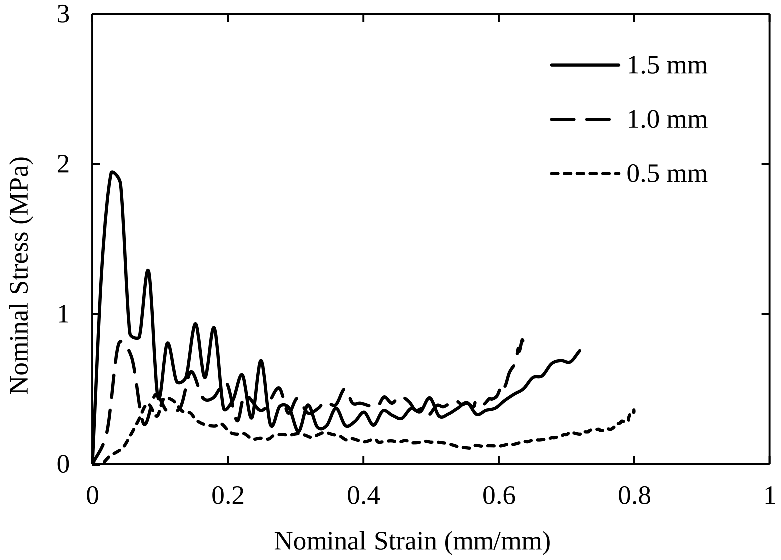

(a)

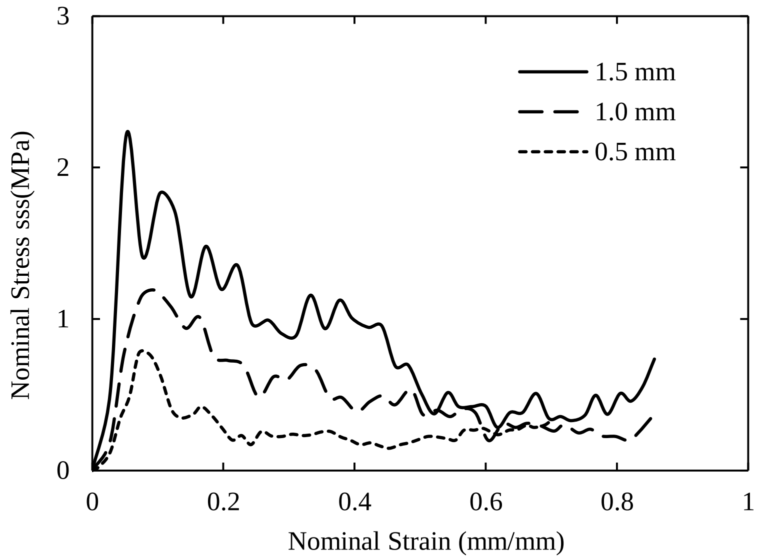

(b)

Figure 12. Typical stress-strain traces following impact compressions tests on (a) the GFRP sandwich panels and (b) the CFRP sandwich panels.

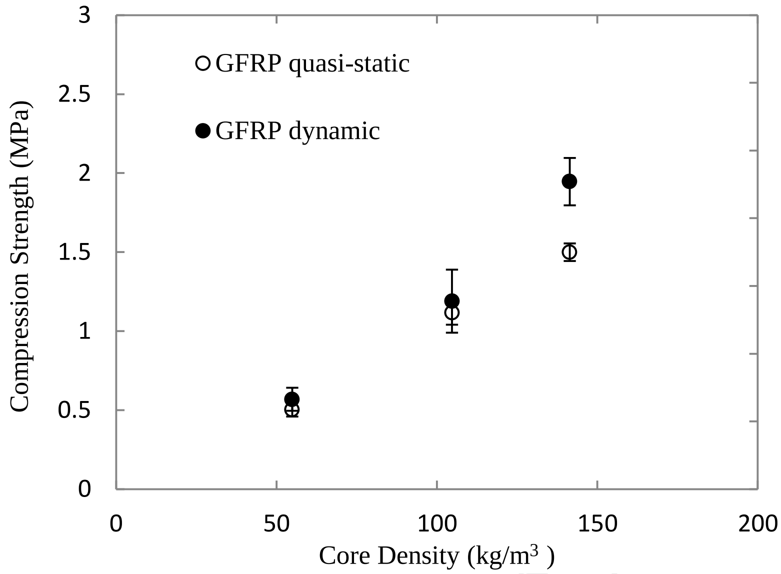

(a) GFRP

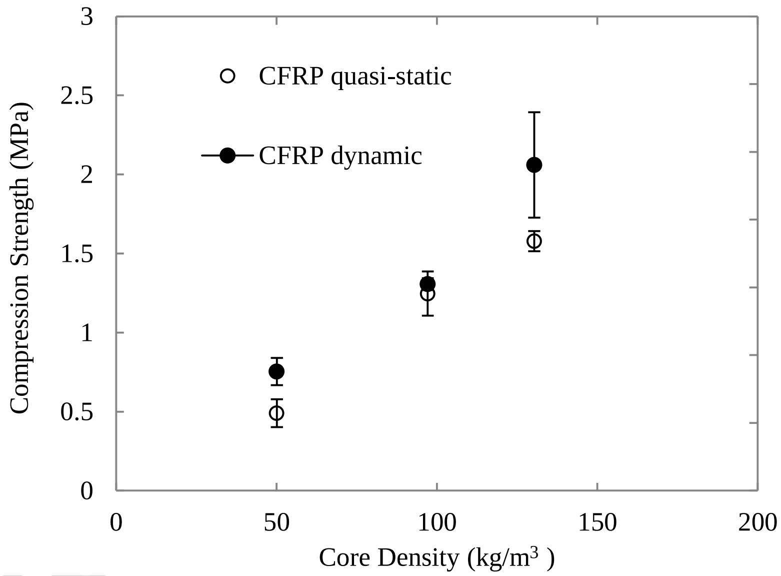

(b) CFRP

Figure 13. Comparison of the impact and quasi-static compression strengths of the (a) GFRP and (b) CFRP panels.

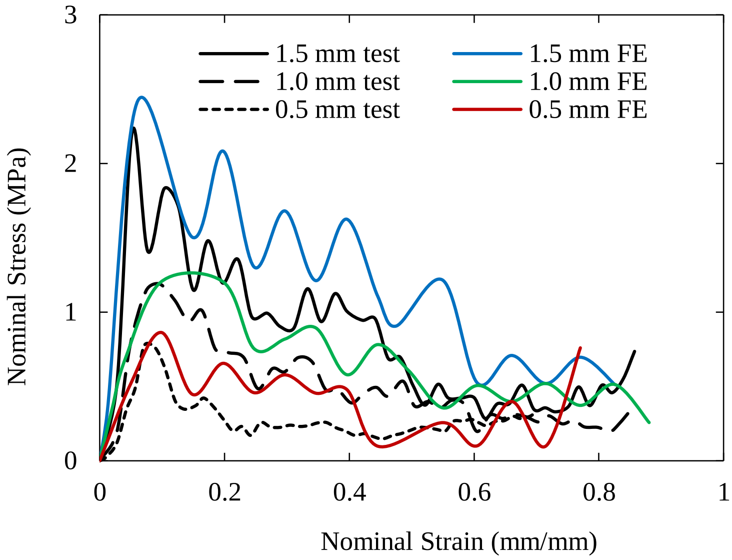

Figure 14. Comparison of the dynamic numerical and experimental stress-strain traces for the CFRP cores.

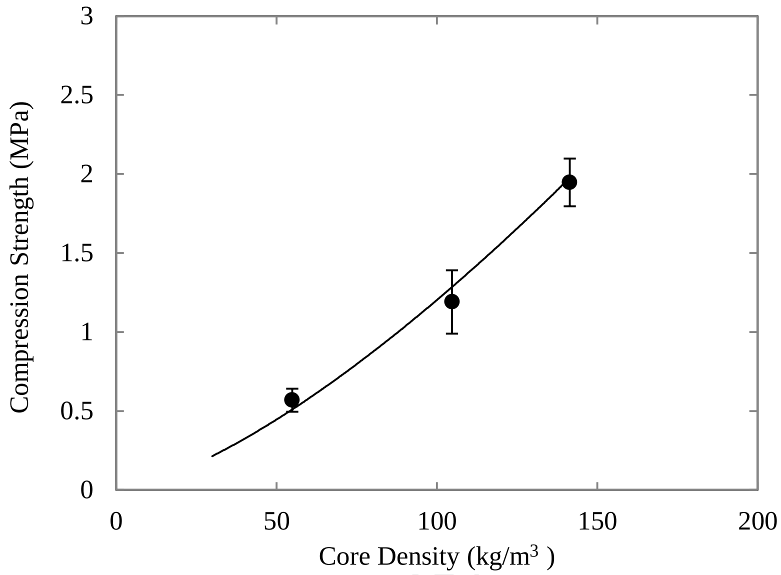

Figure 15. Impact compression strength versus core densities for GFRP samples. The solid line correspond to the FE predictions.